J Mater Sci (2007) 42:19–29
DOI 10.1007/s10853-006-1036-1

Fracture toughness of glass microsphere-filled polypropylene and polypropylene/poly (ethylene terephthalate-co-isophthalate) blend-matrix composites

D. Arencón · J. I. Velasco · V. Realinho · M. Sánchez-Soto · A. Gordillo

Received: 7 September 2005 / Accepted: 19 January 2006 / Published online: 7 November 2006

Abstract The fracture behaviour of glass microsphere-filled polypropylene/poly(ethylene terephthalate-co-isophthalate) blend-matrix composites was investigated in comparison with that of the glass microsphere-filled PP composites. Depending on the deformability displayed by the composite, it was carried out through the linear-elastic fracture mechanics or by applying the *J*-integral concept. The matrix ductility was regulated in the composite through the glass bead surface treatment applied with different silane-coupling agents, as well as with the addition of maleated PP as polymer compatibilizer. Whereas all the composites failed in a brittle manner at moderate impact speed, quasi-brittle fracture behaviour was only observed at low strain rate in composites having high and medium interfacial adhesion level. Results showed that composites containing both aminosilane-treated glass microspheres and maleated PP showed the highest values of fracture toughness. In composites with low adhesion level between matrix and glass beads, the critical *J*-integral value diminished due to the presence of PET.

D. Arencón · J. I. Velasco (✉) · V. Realinho · M. Sánchez-Soto · A. Gordillo
Departament de Ciència dels Materials i Enginyeria Metal·lúrgica, Centre Català del Plàstic, Universitat Politècnica de Catalunya, Vapor Universitari de Terrassa. C. Colom 114, E-08222 Terrassa, Barcelona, Spain
e-mail: jose.ignacio.velasco@upc.edu

Introduction

The fracture behaviour of mineral-filled polypropylene-matrix composites has been studied and their fracture toughness characterized in the recent years [1–9]. The fracture toughness was found dependant on the filler particle morphology, size, surface energy and filler volume concentration.

Among the different fillers for plastics, solid glass microspheres are a special type that induces improved processability and service performance in injection-moulded polypropylene (PP)-matrix composites. Higher thermal conductivity, dimensional stability and small and well-distributed internal stress are three qualities of the glass microsphere-filled PP composites. The fracture behaviour of glass bead-filled PP composites has been studied and the importance of the interfacial adhesion degree has been shown [10–14]. Particle debonding was reported as the main mechanism of energy dissipation [10]. An increase in the glass bead concentration led to a decrease in the values of the composite fracture toughness [11], as well as in both Izod and falling-weight impact strength [12]. A brittle-ductile transition located at 10 vol% of glass microspheres was also reported [13]. In the same paper the surface-treatment with CP-03 silane coupling agent did not result in significant differences in the values of the composite fracture energy. However, surface-treatment of glass microspheres with *N*-(2-(vinylbencylamino)-ethyl)-3-aminopropyl trimethoxy silane led to enhanced adhesion between PP and glass beads, but to a fall in the Izod impact strength [14].

Although short molecules of coupling agents can create strong bonds with the glass microsphere surface, they usually do not form either chemical bonds with

the PP molecules or physical entanglements that cause improvement in the PP cohesive strength. For this reason, high molecular-weight adhesive agents are preferred, which create strong bonds with the filler surface as well as physical entanglements with the polymer matrix. The most usually employed are PP graft-copolymers containing polar groups [15–19]. Nevertheless, it has been recently proposed to employ of some polar thermoplastics such as polyamide [20], polycarbonate [21] and polyethyleneterephthalate [22–25] as efficient interfacial agents because of their affinity to high-polarity particle surfaces. Bearing in mind this idea, homologous series of glass microsphere-filled PP and PP/PET blend composites were prepared with the aim of investigating possible beneficial effects due to the presence of PET on the PP composite fracture toughness. In these composites, a strong dependence of the tensile properties on the adhesion degree between matrix and filler was found [24, 25]. In the present paper, the fracture toughness of four series of glass microsphere-filled PP and PP/PET composites with different ductility degrees promoted by different interfacial adhesion levels has been characterized by application of linear-elastic fracture mechanics (LEFM) and *J*-integral concepts.

Materials and specimens

Polypropylene was provided by *Repsol-YPF* (Puertollano, Spain). It was a homopolymer grade (*Isplen PP050*) with melt flow index (conditions: 230 °C and 2,160 g) 5.0 g/10 min. Solid glass microspheres (*Sovitec Ibérica*, Castellbisbal, Spain) with average particle size of 20 μm were employed as filler. *Eastman Chemical* (Madrid, Spain) supplied a commercial grade (*Epolene G-3003*) of maleated polypropylene (MAPP) of acid number 8. *Extrupet EW36* was a poly(ethylene terephthalate-co-isophthalate) manufactured by *Catalana de Polímers S.A.* (El Prat de Llobregat, Spain), with intrinsic viscosity 0.8 dl/g.

PP/PET blends were prepared by melt extrusion with the composition shown in Table 1. To promote compatibillization between both polymers MAPP was added, resulting in a blend PP/MAPP/PET. The non-compatibilized blend PP/MAPP and the neat polypropylene were also extruded in the same conditions for comparison proposals.

The nomenclature and composition of the composites are shown in Tables 1, 2. All the composites had 50% by weight of glass microspheres. Both untreated and silane treated glass beads were employed. Three

Table 1 Polymer matrix reference and composition expressed in percentages by weight

Matrix reference	A	B	C	D
Composition	PP (100)	PP/MAPP (97/3)	PP/PET (95/5)	PP/MAPP/PET (92/3/5)

different silane coupling agents were used for glass beads surface treatment (Table 2). The procedure used to homogeneously coat the glass bead surface with the silane, as well as the preparation of the composites is described elsewhere [25].

Prismatic specimens of nominal dimensions $9 \times 18 \times 78$ mm^3 were injection-moulded using a Meteor 440/90 (Mateu & Solé, Spain) injection-moulding machine and a specially designed two-cavity mould. The temperature profile in the injection cylinder was 150–220–230–240–250 °C, the mould temperature was 60 °C and the nominal injection pressure was 90 MPa.

Single-edge notched three-point bend (SENB) fracture specimens were prepared by inserting notches centrally on the narrowest side of the prismatic bars, using a 45° V notch broaching tool. These blunt notches were sharpened with a single cut from a razor blade in order to get an initial sharp crack.

Testing

Linear-elastic fracture mechanics (LEFM) tests

To determine the LEFM parameters, fracture tests were carried out at room temperature (20 °C ± 2) and at two different strain rate levels, employing a 72 mm span on the above described SENB specimens. First, low rate tests were carried out in a universal mechanical testing machine (Galdabini Sun 2500) at a cross-head speed of 1 mm/min. The specimens had different crack lengths, ranging between 8.4 and 9.0 mm. Second; moderate high rate tests were carried out on an instrumented Charpy impact pendulum (CEAST, Italy) at an impact speed of 0.5 m/s. The analysis of the results from the low-rate tests showed independency of the LEFM parameters with the initial crack length. Therefore, in the high-rate impact tests, a constant initial crack length of 9.0 mm was preferred.

According to the LEFM principles, the critical stress intensity factor (K_C) and the critical strain energy release rate (G_C) may be calculated for SENB geometry through the following equations:

Table 2 Reference and type of silane on the glass bead surface

GB surface treatment reference	Silane coupling agent	Commercial name
1	None	–
2	3-mercaptopropyl trimethoxy silane	A-189[b]
3	*N*-(2-aminoethyl)-3-aminopropyl trimethoxy silane	Z-6020[a]
4	*N*-(2-(vinylbencylamino)-ethyl)-3-aminopropyl trimethoxy silane	Z-6032[a]

Organosilanes supplied by (a) Dow Corning and (b) Witco

$$K_C = \frac{P_{5\%} Sf}{BW^{3/2}} \quad (1)$$

$$G_C = \frac{U_{5\%}}{BW\Phi}. \quad (2)$$

$P_{5\%}$ and $U_{5\%}$ are the measured force and the stored strain energy in the 5% offset load, according to the ESIS testing protocol [26]. The energy ($U_{5\%}$) was corrected by subtracting the rods indentation contribution. For that, indentation tests were carried out in each composite. In the above equations, B and W are, respectively, the thickness and width of the specimen, S is the span, whereas f and Φ are two dimensionless geometry calibration factors [26]. In addition to the experimental value of G_C, a calculated G_C value can also be obtained form K_C and Young's modulus (E) experimental values, through the well-known expression for plane strain conditions at the crack tip:

$$G_C^{calc} = \frac{K_C^2}{E}(1 - \nu^2). \quad (3)$$

Here, ν indicates the Poisson ratio.

J-integral tests

Three-point bending *J*-integral fracture tests were conducted at a crosshead speed of 1 mm/min. Like the LEFM fracture tests, the experiments were done at room temperature (20 ± 2 °C).

According to the elastic–plastic fracture mechanics (EPFM), for SENB specimens with a span to width ratio (S/W) of 4 the *J*-integral can be calculated as:

$$J = \frac{2U}{B(W - a_0)}\left(1 - \frac{(1.5 - \Delta a)}{(W - a_0)}\right) \quad (4)$$

U represents the energy to initiate and propagate the crack, a_0 is the initial crack length and Δa is the crack stable extension. *J*-integral determinations were performed using a multiple specimen resistance-cure (*R*-curve) methodology. To construct the *R*-curve (plot of J vs. Δa), a set of identical SENB specimens with nominal values of a_0=10 mm were loaded monotonically to different deflections, all less than that to give total failure, to obtain different levels of stable crack extension (Δa), and then fully unloaded. For each specimen, the J value was calculated from the energy up to that deflection (U), after subtracting the rods indentation contribution, using Eq. 4. To develop the stable crack extension in the specimens, a drop of India ink was placed into the initial crack tip before the loading. At the finish of the test, once the ink was dried, the specimens were fractured at impact speed and so the stable crack growth was developed by the dried ink on the fracture surface. Measurement of the final crack front from the fracture face was carried out using a projector of profiles (Nikon 6C).

To construct *R*-curves, the J–Δa points were fitted according to two protocols. On one hand, the recommendations of ASTM E813-81 [27] procedure were followed. The J–Δa points in the *R*-curve were located between two exclusion lines, which were parallel to the blunting line of the crack tip:

$$J = 2m_{pcl}\Delta a\sigma_y. \quad (5)$$

Here m_{pcl} is the plastic constraint factor, equal to $\sqrt{3}$ for plastic materials [28, 29], and σ_y is the tensile yield strength. The parallel exclusion lines are located at $\Delta a = 0.006(W - a)$ and $\Delta a = 0.06(W - a)$, respectively. According to ASTM E813-81, the valid data points are then linearly regressed to obtain the *R*-curve, and the crack initiation point is then defined as the intersection of the *R*-curve with the blunting line, which gives the J_{IC} value.

On the other hand, the ESIS procedure [30] was followed, where the valid J–Δa points are located between $\Delta a = 0.05$ mm and $\Delta a = 0.1(W - a)$ parallel lines, and after they are fitted with a power-law function. The crack initiation point is defined as the intersection of the *R*-curve with the abscise $\Delta a = 0.2$ mm.

Fractography

The fracture surfaces were examined by scanning electron microscopy (SEM) in order to investigate the morphological aspects associated with the deformation

and fracture processes. A JSM-820 (JEOL) scanning electron microscope was employed, after gold was sputtered onto the surface to make it conductive.

Results and discussion

LEFM fracture analysis

Low-rate fracture

From a macroscopic point of view, only the composites with strong interfacial adhesion displayed brittle fracture at 1 mm/min, whereas the composites with poor adhesion between matrix and glass surface displayed ductile fracture. As illustrated in Fig. 1, the load–displacement (P–d) linearity requirement usually accepted for fracture behaviour of plastics under LEFM conditions is $P_{max}/P_{5\%} < 1.1$, that is, a 10% of non-linearity is accepted for these materials. Six composites (B3, B4, D1, D2, D3 and D4) among those studied in this research satisfied this requirement (Table 3). On the one hand, in composites B3 and B4, the strong interfacial adhesion was achieved by functionalizing the polypropylene matrix with poly (propylene-co-maleic anhydride) (MAPP) as well as by using glass microspheres surface-treated with aminosilane (Z-6020) and vinylbenzyl cationic silane (Z-6032). On the other hand, in composites D1, D2, D3 and D4 strong adhesion was achieved exclusively by using the compatibilized PP/PET blend as matrix, independently of the glass surface nature [24, 25]. That is, both untreated and mercaptosilane-treated glass beads composites, which did not accomplish the LEFM statements in PP-based composites, did it in compatibilized PP/PET blend-based ones (Fig. 2). This behaviour is explained on a basis of the following combined effects: the tendency of PET to bond to the glass surface and the good compatibilization between both polymers, promoted by MAPP.

To determine the fracture toughness at 1 mm/min, the experimentally recorded values of $P_{5\%}$ and $U_{5\%}$ were linearized according to Eqs. 1, 2, and from the slope of these plots (Fig. 3) values of K_C and G_C could be determined as fracture parameters independent of the initial crack length. The results are shown in Table 3. Two different levels of fracture toughness were observed. On one hand, high K_C values ranging between 2.2 and 2.4 MPa $m^{1/2}$ were displayed by composites (B3, B4, D3 and D4) containing glass microspheres treated with silanes Z-6020 and Z-6032. On the other hand, low values of K_C close to 1.7 MPa $m^{1/2}$ were found in composites D1 and D2. From these results, it can be concluded that aminosilanes are efficient coupling agents to enhance the fracture toughness of glass microspheres/PP composites with high interfacial adhesion. The amine groups in the silane would be the responsible of this improvement, by reaction with the carboxyl groups of MAPP and/or PET.

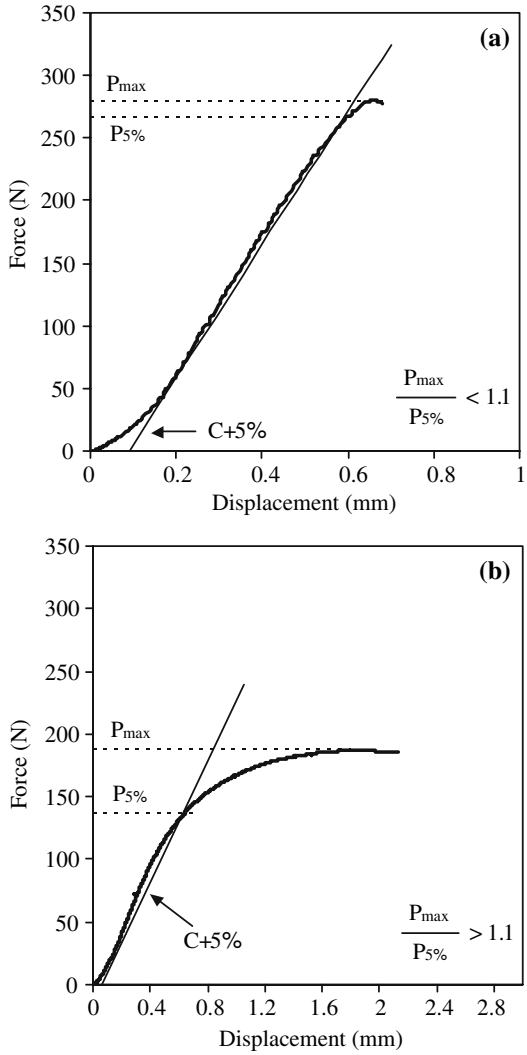

Fig. 1 Force–displacement curves of (**a**) D2 and (**b**) A2 composites at 1 mm/min. a_0=9.0 mm

It must be noted that the size criterion (Eq. 6), usually used to ascertain if the fracture parameters have been determined under plane strain stress state, was not fulfilled by composites containing Z-6032 silane-treated glass beads (composites B4 and D4)

$$B(W - a_0) > \frac{2.5K_C^2}{\sigma_y^2}. \quad (6)$$

In addition, a similar trend to that of the K_C values was observed in G_C. Both values of the fracture energy, the

Table 3 LEFM analysis at low strain rate. Standard deviation into brackets

Composite	Interfacial adhesion level	$P_{max}/P_{5\%}$	K_C (MPa m$^{1/2}$)	G_C (kJ/m^2)	G_C^{calc} (kJ/m^2)	2.5 K_C^2/σ_y^2(mm)
A1	Low	>1.1	–	–	–	–
A2	Low	>1.1	–	–	–	–
A3	Low	>1.1	–	–	–	–
A4	Medium	>1.1	–	–	–	–
B1	Medium	>1.1	–	–	–	–
B2	Medium	>1.1	–	–	–	–
B3	High	<1.1	2.2 (0.1)	1.4 (0.1)	1.1	8.8
B4	High	<1.1	2.4 (0.1)	1.8 (0.2)	1.3	10.5
C1	Low	>1.1	–	–	–	–
C2	Low	>1.1	–	–	–	–
C3	Low	>1.1	–	–	–	–
C4	Low	>1.1	–	–	–	–
D1	High	<1.1	1.7 (0.1)	0.9 (0.1)	0.7	6.5
D2	High	<1.1	1.7 (0.1)	0.9 (0.1)	0.8	6.8
D3	High	<1.1	2.2 (0.1)	1.2 (0.1)	1.2	8.9
D4	High	<1.1	2.3 (0.1)	1.5 (0.1)	1.4	10.0

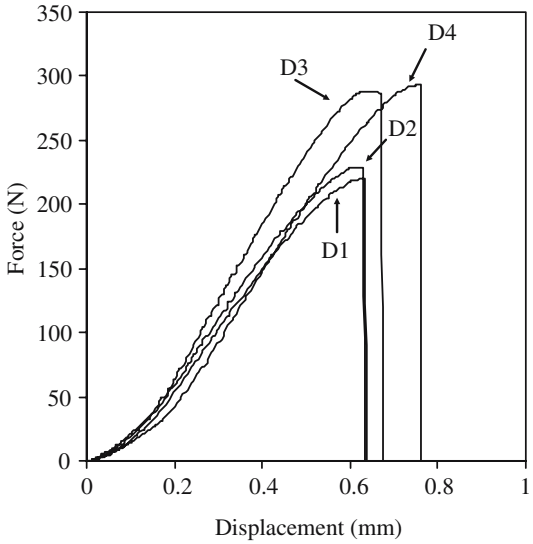

Fig. 2 Force–displacement curves of samples with matrix composition PP/MAPP/PET

experimentally determined (G_C) and the calculated (G_C^{calc}) were found to be very alike, and they followed the same trend with the material composition.

The microscopic analysis of the fracture surfaces carried out by SEM revealed microplasticity developed by the polymer matrix, which was present in all the composites fractured at 1 mm/min. This feature resulted much more evident in the fracture of composites displaying a medium adhesion level (Fig. 4a) than in composites where the glass surface was strongly adhered to the matrix (Fig. 4b, c). Although the linearity requirement was clearly accomplished by these composites having a high interfacial adhesion level, their low-rate fracture took place with some extent of matrix microplasticity, as it can be appreciated in the micrographs of Fig. 4b,c.

High-rate fracture

The common feature of the composite fracture behaviour by impact was that all the studied composites

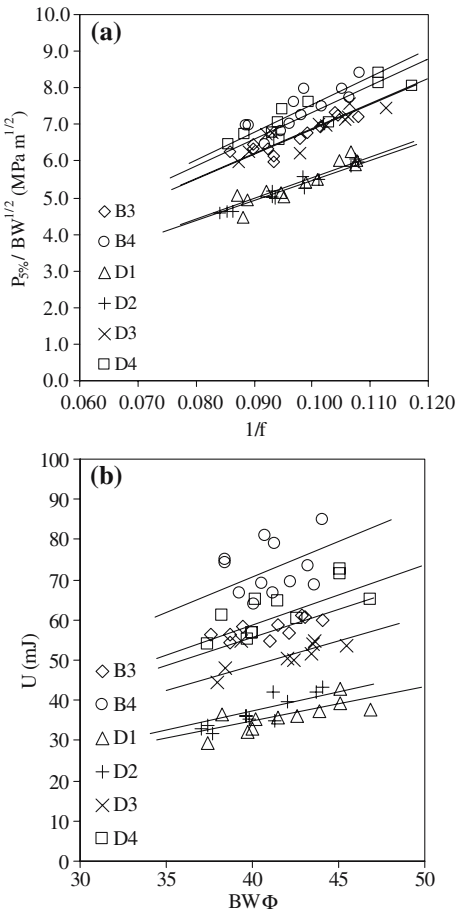

Fig. 3 Linearization of (**a**) $P_{5\%}$ and (**b**) $U_{5\%}$ in order to obtain K_C and G_C fracture parameters

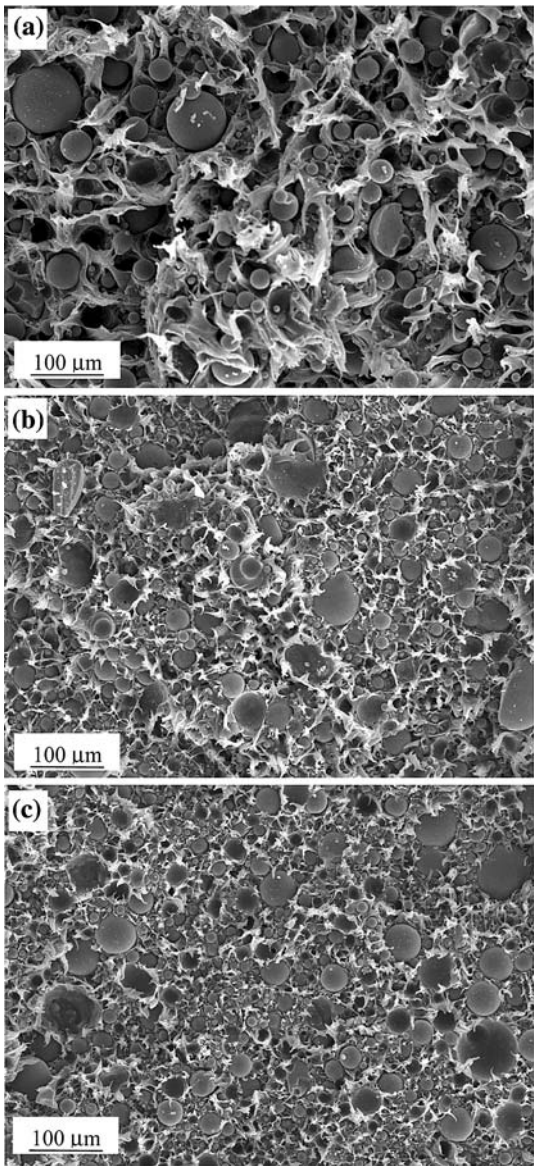

Fig. 4 Fracture surfaces of composites (**a**) B2, (**b**) B3 and (**c**) D2 after testing at 1 mm/min

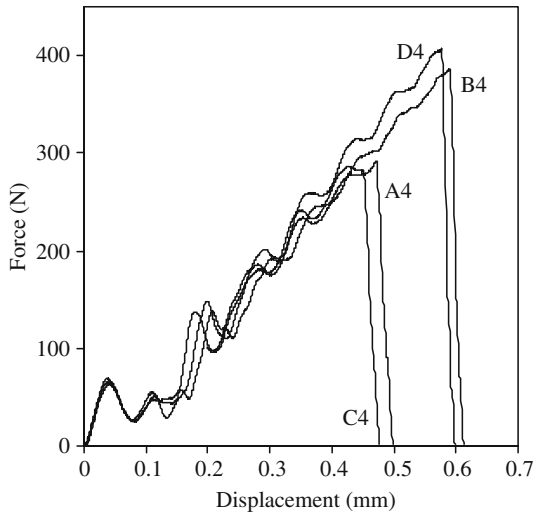

Fig. 5 Impact force–displacement curves of composites with glass beads treated with silane Z-6032

fractured in a brittle manner. An example of the force–displacement curves recorded by the impact tests is shown in Fig. 5. Despite the presence of dynamic effects, all the composite materials were able to fulfil the linearity criteria ($P_{max}/P_{5\%} < 1.1$). The obtained results have been compiled in Table 4. Again, two levels of fracture toughness were observed. On one hand, K_C values ranging between 2.8 and 3.1 MPa $m^{1/2}$ were displayed by the composites having MAPP and glass beads treated with both types of aminosilanes (Z-6020 and Z-6032) independently of the PET presence (composites B3, B4, D3 and D4). On the other hand, values of K_C comprised between 2.3 and 2.5 MPa $m^{1/2}$ were found in the rest of composites. The higher interfacial adhesion degree in the composite resulted in higher fracture toughness. The fracture energy values of composites with aminosilane-treated glass beads were again the highest (G_C = 1.6–2.2 kJ/m^2). The calculated and experimental fracture energy values showed a similar trend.

Two composites displaying low adhesion level (A1 and A2) gave also high G_C values (1.9 and 2.2 kJ/m^2). In these composites the extensive microspheres debonding (Fig. 6a) could act as the responsible micromechanism of the fracture energy increase. After fractography analysis by SEM, there was no evidence in any composite of microplasticity developed by the polymer matrix before or during the crack propagation by impact. Depending on the interfacial adhesion level, different fracture patterns were displayed. So, adhesive fracture occurred in the composites with low interfacial adhesion (Fig. 6a) and cohesive fracture through the matrix in the composites with high interfacial adhesion (Fig. 6c). An intermediate pattern between adhesive and cohesive fracture was displayed by composites having medium interfacial adhesion level (Fig. 6b).

Different values of the fracture parameters are found in the literature for PP and PP-based materials. When the former results on glass microsphere-filled polypropylene and polypropylene/poly (ethylene terephthalate-co-isophthalate) blend-matrix composites are compared with those reported in [31] (K_{IC} = 1.9 MPa $m^{1/2}$, G_{IC} = 2.7 kJ/m^2) and in [2] (K_{IC} = 1.9 MPa $m^{1/2}$, G_{IC} = 2.10 kJ/m^2) for injection-moulded homopolymer PP determined at moderate impact rate, one can conclude that the addition of 50 wt% of glass microspheres slightly reinforce the PP fracture toughness.

Table 4 LEFM analysis data at impact speed. Standard deviation is into brackets

Composite	$P_{max}/P_{5\%}$	K_C (MPa $m^{1/2}$)	G_C (kJ/m^2)	G_C^{calc} (kJ/m^2)	$2.5K_C^2/\sigma_y^2$ (mm)
A1	<1.1	2.5 (0.2)	1.9 (0.3)	1.2	26.7
A2	<1.1	2.5 (0.1)	2.1 (0.3)	1.2	29.2
A3	<1.1	2.4 (0.2)	1.3 (0.3)	1.2	22.7
A4	<1.1	2.4 (0.1)	1.1 (0.1)	1.0	14.6
B1	<1.1	2.6 (0.1)	1.5 (0.3)	1.4	13.5
B2	<1.1	2.2 (0.1)	1.0 (0.1)	0.9	15.0
B3	<1.1	2.8 (0.2)	1.6 (0.3)	1.4	10.7
B4	<1.1	2.9 (0.2)	2.1 (0.2)	1.6	11.6
C1	<1.1	2.4 (0.1)	1.3 (0.1)	0.9	27.7
C2	<1.1	2.3 (0.1)	1.3 (0.2)	1.0	28.8
C3	<1.1	2.5 (0.1)	1.6 (0.1)	1.1	31.7
C4	<1.1	2.3 (0.1)	1.0 (0.2)	0.9	21.1
D1	<1.1	2.3 (0.2)	1.0 (0.1)	0.8	7.3
D2	<1.1	2.1 (0.1)	0.9 (0.1)	0.7	6.7
D3	<1.1	2.8 (0.2)	1.8 (0.1)	1.2	9.8
D4	<1.1	3.1 (0.1)	2.2 (0.1)	1.6	13.6

Such reinforcement effect results more remarkable as higher is the interfacial adhesion level in the composite. In addition, a reduction of the fracture energy accompanies the fracture toughness reinforcement. This is explained by the slight increase in the K_C values, which is not enough to compensate the dramatic increase of the Young's modulus in the composite [25], respect to the pure PP.

EPFM fracture analysis

J–R curves

The elastoplastic fracture analysis based on *J*-integral values was performed on both non-functionalized PP and non-compatibilized PP/PET blend-matrix composites (A and C series). These composites had low interfacial adhesion level because of the no presence of MAPP in the polymer matrix, and they displayed stable ductile fracture at 1 mm/min. Thus, the *J–R* curves could be constructed for these samples. Examples of these fracture curves are shown in Fig. 7, and the typical appearance of the crack front, as revealed by the ink on the fracture surface of a tested specimen, can be seen in Fig. 8. All the tested composites fulfilled the specimen thickness criterion usually applied to guarantee the crack growth controlled by *J*-integral in metallic SENB specimens:

$$B(W - a_0) > \frac{25J_C}{\sigma_y}. \quad (7)$$

The *J–R* curves constructed from the tests data are shown in Figs. 9, 10. Both linear and power law-data fits were realized according to ASTM E813-81 (Fig. 9) and ESIS 2000 (Fig. 10), respectively. The numerical results of these analyses are compiled in Tables 5 and 6, respectively. The comparison of results from both procedures indicated that the ASTM E813-81 method resulted very restrictive for the composites studied here, as concluded in sight of the very low *J*-integral critical values (J_{IC}) obtained for the composites of the series C. The *J*-integral critical values ($J_{0.2}$) obtained according to the ESIS protocol for plastic materials, resulted more reasonable.

Focusing on the $J_{0.2}$ values, the results indicated that the aminosilane Z-6020 treatment on the glass surface reduced the composite fracture resistance ($J_{0.2}$ = 3 kJ/m^2) if compared with untreated and mercaptosilane-treated glass bead-filled composites ($J_{0.2}$ = 5 kJ/m^2). Such difference should be related to a slightly improved interface in A3 sample promoted by the aminosilane, which would limit the plastic flow of the matrix microligaments between contiguous microspheres, thus lowering the energy consumption before the crack growth onset. The non-compatibilized PP/PET matrix composites (series C) resulted in lower $J_{0.2}$ values with regard to the PP matrix composites (series A). Here, both the fine PET droplets dispersed within the PP and the fraction of PET encapsulating the glass bead surface [24] would limit the matrix deformability, as indicated by the values of strain at break from tensile tests [25], giving rise to less dissipation of energy before the crack propagation.

It would be interesting to compare the obtained *J* critical values of the composites with that of the unfilled PP. Nevertheless, the fracture behaviour of unfilled homopolymer polypropylene at low strain rate displays ductile instability at low crack extension. It has been reported that it takes place in testing specimens

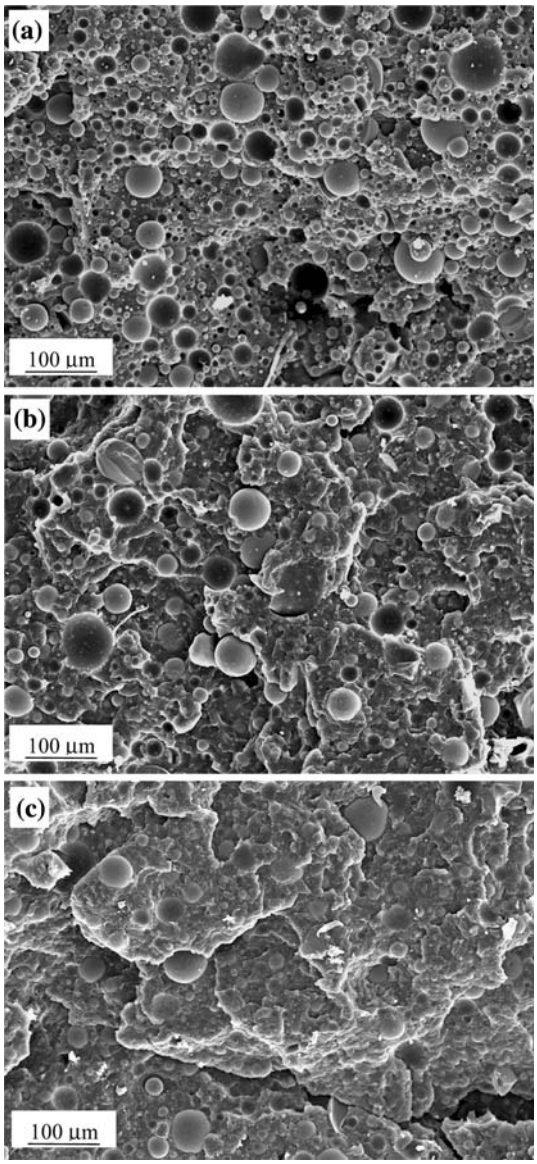

Fig. 6 Fracture surfaces obtained by impact tests. (**a**) A1, (**b**) B1 and (**c**) D1

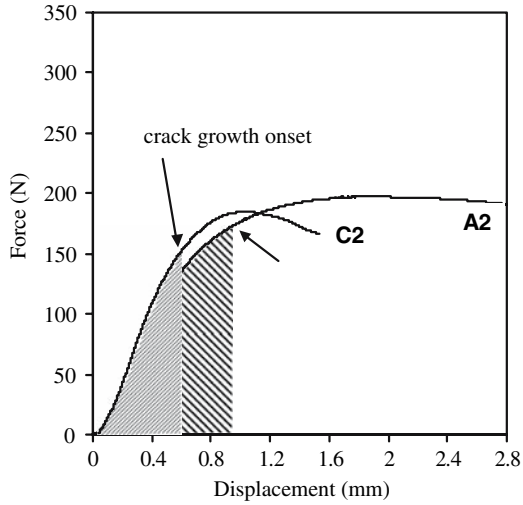

Fig. 7 Force–displacement curves of A2 and C2 composites at 1 mm/min. a_0=10.0 mm

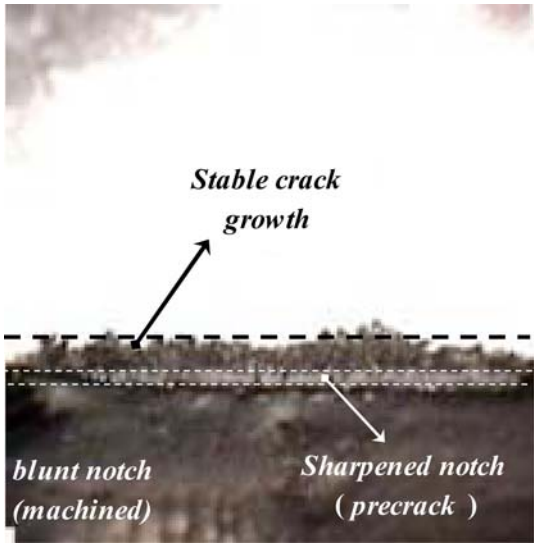

Fig. 8 General aspect of SENB samples after testing employed for *J*-integral critical value determination

of thickness higher than 1 mm [32]. Thus, *J*–*R* curves are not possible to construct for this material, and only estimations of its critical *J*-integral value can be realised (i.e. J_{IC} = 6.57 kJ/m^2 [2]).

Fracture mechanisms

The addition of particulate mineral fillers into homopolymer PP usually eliminates the ductile instability, making stable the crack propagation even with the addition of a very low concentration of filler particles [3]. In this sense, the calculated values of the composite tearing modulus (T_M) were in good agreement with the stability of the crack propagation observed. The condition given by Paris [33] for steady-state tearing was fulfilled:

$$T_M = \frac{2(W - a_0)S}{W^3} > 2. \quad (8)$$

After the fractographic analysis carried out (Fig. 11) it was corroborated that the main micromechanisms involved in the composite low-rate fracture were the microsphere debonding and the further matrix plastic flow. The poor microsphere/matrix interfacial adhesion was the responsible factor of particle debonding,

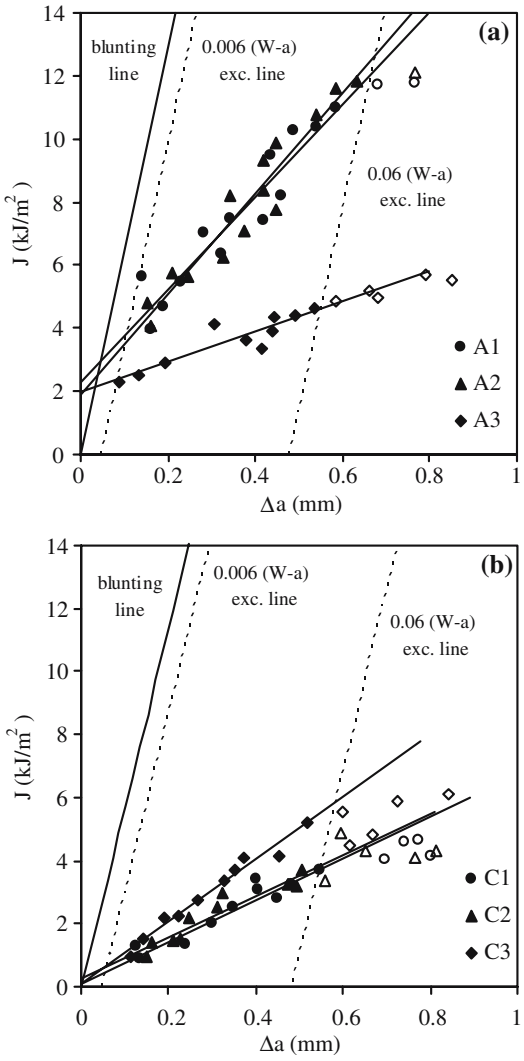

Fig. 9 Experimental *J*–*R* plots according to ASTM E813–81, of (**a**) A composites and (**b**) C composites

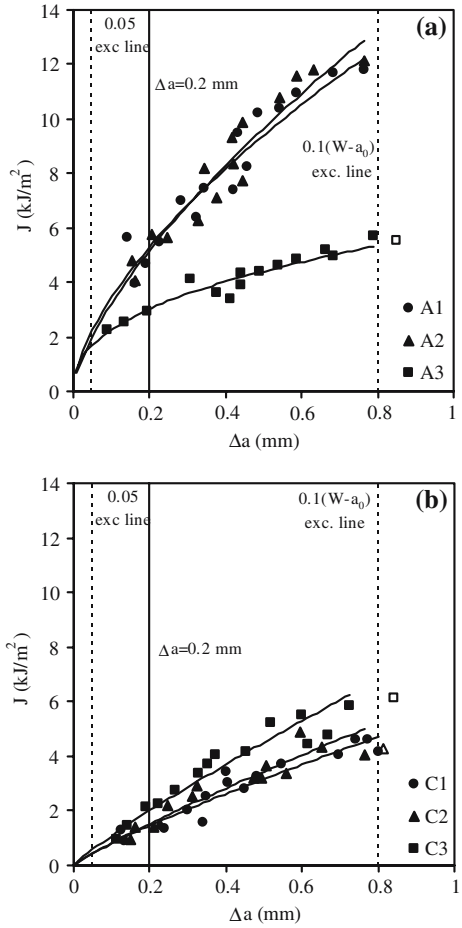

Fig. 10 Experimental *J*–*R* plots according to ESIS 2000, of (**a**) A composites and (**b**) C composites

whereas the presence of PET constrained the matrix deformability. In general, in these composites the microsphere debonds from the matrix at a low stress level; then, the matrix microligaments can be drawn until fracture by tearing. Some kind of ''crests'' appears on the fracture surface, which are the drawn matrix microligaments. This pattern is clearly observed in micrographs of A1 and A2 samples (Fig. 11a, b), and it resulted in the highest *J*-integral critical value. The size (length) of the crests appreciated in the fracture surface of A3 sample (Fig. 11c) is lower as a consequence of the lower plastic flow extension, which would lead to a reduction of the plastic energy involved during the crack propagation. Therefore, the fall in the critical *J*-integral value of A3 composite is in good agreement with the fracture surface analysis. The presence of PET [34] could explain the reduction of the ductile tearing observed by SEM in the composites of series C (Fig. 11d–f), when compared with samples of A series. Fracture surfaces of these composites were very similar between each other.

Conclusions

The fracture behaviour of glass microsphere-filled polypropylene and polypropylene/poly (ethylene terephthalate-co-isophthalate) blend-matrix composites was comparatively investigated. At low strain rate (1 mm/min) composites with medium and high interfacial adhesion displayed quasi-brittle fracture, although only the latter fulfilled LEFM requirements. Composites with both MAPP and glass beads treated with aminosilane showed the highest values of fracture toughness (K_{IC}) and fracture energy (G_{IC}). Brittle fracture was observed, and the LEFM fracture toughness was measured, in all the studied composites at moderate impact speed (0.5 m/s).

Table 5 *J*-integral parameters from the analysis according to the ASTM E813 standard

Composite	J–Δa linear fit	Blunting line J_b=2 m_{pl} σ_y Δa	J_{IC} (kJ/m^2)	25 J_{IC}/σ_y (mm)	T_M
A1	$J = 14.63\Delta a + 2.31$	$J_b = 64.05\Delta a$	3.0	4.1	156.9
A2	$J = 15.93\Delta a + 1.90$	$J_b = 58.44\Delta a$	2.6	3.6	202.8
A3	$J = 4.84\Delta a + 1.96$	$J_b = 66.86\Delta a$	2.1	2.9	42.2
C1	$J = 6.63\Delta a + 0.08$	$J_b = 57.30\Delta a$	0.1	0.1	85.3
C2	$J = 6.55\Delta a + 0.28$	$J_b = 56.08\Delta a$	0.3	0.4	80.4
C3	$J = 9.91\Delta a + 0.08$	$J_b = 57.12\Delta a$	0.1	0.1	117.9

Table 6 *J*-integral parameters from the analysis according to the ESIS

Composite	J–Δa potential fit	$J_{0.2}$ (kJ/m^2)	25 $J_{0.2}/\sigma_y$ (mm)	T_M
A1	$J = 14.45\Delta a^{0.62}$	5.3	7.2	176.8
A2	$J = 15.48\Delta a^{0.68}$	5.2	7.6	224.0
A3	$J = 5.86\Delta a^{0.41}$	3.0	3.9	54.3
C1	$J = 5.68\Delta a^{0.84}$	1.5	2.2	79.3
C2	$J = 6.03\Delta a^{0.84}$	1.5	2.4	80.1
C3	$J = 8.01\Delta a^{0.85}$	2.0	3.1	102.7

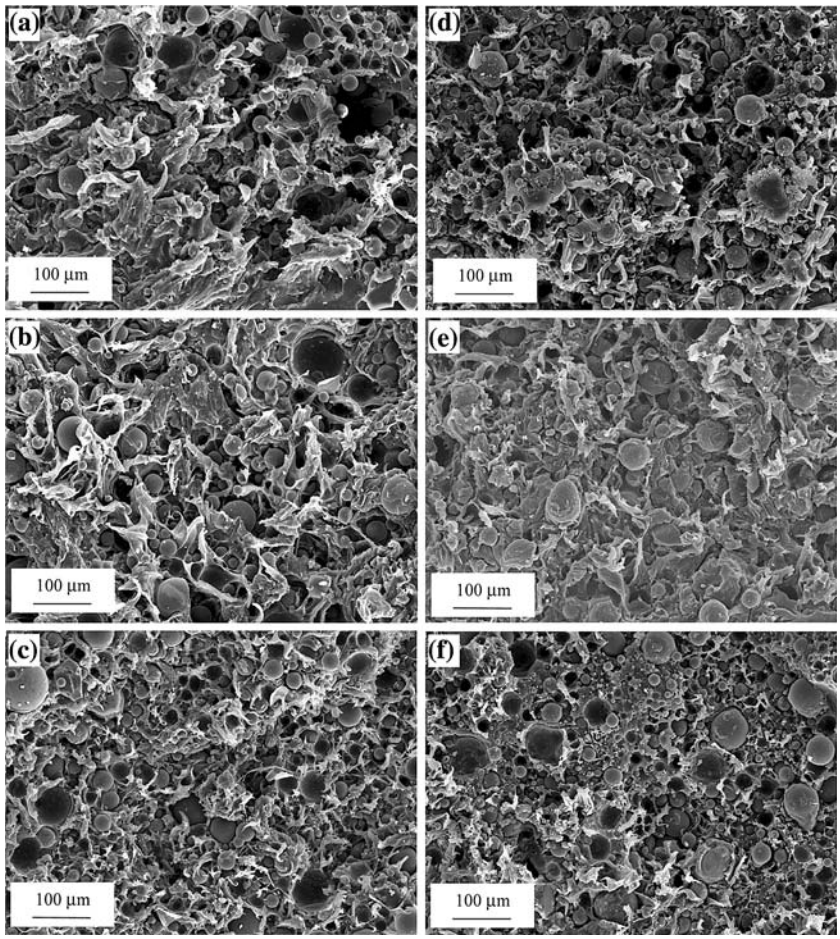

Fig. 11 Fracture surfaces of *J*-integral specimens of composites (**a**) A1, (**b**) A2, (**c**) A3, (**d**) C1, (**e**) C2 and (**f**) C3

The fracture of composites with low interfacial adhesion level was ductile at 1 mm/min, and it could be studied through *J*-integral analysis. The addition of PET into the composites resulted in a lower fracture toughness, probably because of poor compatibility between both polymers. Different effects were

observed depending on both the silane-treatment applied on the glass microsphere surface and on the matrix composition.

Acknowledgements Authors thank to the Spanish Ministry of Science (MEC) for financial support of MAT2004-01563 project. D. Arencón also thanks to the CIRIT (Government of Catalonia, Spain) for a doctoral fellowship.

References

1. Karger-Kocsis J (1995) In: Karger-Kocsis J (ed) Polypropylene: structure, blends and composites. Chapman & Hall, London
2. Velasco JI, De Saja JA, Martínez AB (1997) Fatigue Frac Eng Mater Struct 20:659
3. Velasco JI, Morhain C, Arencón D, Santana OO, Maspoch MLL (1998) Polym Bull 41:615
4. Velasco JI, Morhain C, Maspoch MLI, Santana OO (1998) In: Brown MW, de los Rios ER, Miller KJ (eds) ECF 12 – Fracture from Defects. EMAS Publishing, Wentworth
5. Morhain C, Velasco JI (2002) J Mater Sci 37(8):1635
6. Labour T, Vigier G, Seguela R, Gauthier C, Orange G, Bomal Y (2002) J Polym Sci Part B Polym Phys 40(1):31
7. Szabo JS, Czigany T (2003) Polym Testing 22(6):711
8. Dasari A, Misra RDK (2004) Acta Mater 52(6):1683
9. Gong G, Xie BH, Yang W, Li ZM, Zhang WQ, Yang MB (2005) Polym Testing 24(4):410
10. Asp LE, Sjöngren BA, Berglund LA (1997) Polym Comp 18:9
11. Tsui CP, Tang CY, Lee TC (2002) In: Ligtning Source Inc. (ed) Fracture mechanics testing methods for polymers adhesives and composites. Elsevier Science, Kidlington, pp 395–406
12. Sjöngren BA, Berglund LA (1997) Polym Comp 18:1
13. Liang JZ, Li RKY (1999) Polymer 40:3191
14. Davies LC, Sothern GR, Hodd KA (1988) Plastics Rubb Process Appl 5:9
15. Stamhuis JE (1988) Polym Comp 9:72
16. Xavier XF, Schultz JM, Friedrich K (1990) J Mater Sci 25:2411
17. Felix JM, Gatenholm P (1991) J Appl Polym Sci 50:699
18. Bikiaris D, Matzinos P, Larena A, Flaris V, Panayiotou CJ (2001) J Appl Polym Sci 81:701
19. García-Martínez JM, Laguna O, Areso S, Collar EP (2001) J Appl Polym Sci 81:625
20. Ulrich M, Caze C, Laroche P (1998) J Appl Polym Sci 67:201
21. Noh CH, Yoon BS, Suh MH, Lee SH (2001) Polymer 42:2695
22. Velasco JI, Ardanuy M, Miralles L, Ortiz S, Maspoch MLI, Sánchez-Soto M, Santana O (2005) Macromol Symp 221:63
23. Arencon D, Maspoch MLI, Velasco JI (2003) Macromol Symp 194:225
24. Arencón D, Velasco JI, Rodríguez-Pérez MA, De Saja JA (2004) J Appl Polym Sci 94(4):1841
25. Arencón D, Velasco JI, Ardanuy M, Martinez AB J Mater Sci (in progress)
26. ESIS Technical Committee 4 (1990) A linear-elastic fracture mechanics (LEFM) standard for determining K_c and G_c for plastics. Testing protocol. European Structural Integrity Society, March 1990
27. ASTM Standard E813-81 (1981) Annual book of ASTM Standards. Part 10. American Society for Testing and Materials, Philadelphia, PA, p 810
28. Irwin GR (1960) In Proceedings of the Seventh Sagamore Ordnance Materials Conference, vol. IV. Syracuse University, New York, pp 63–78
29. Irwin GR (1964) Appl Mater Res 3:65
30. ESIS Technical Committee 4 (2000) A testing protocol for conducting J–R curve tests on plastics. European Structural Integrity Society, March 2000
31. Casiragui T, Castiglioni G, Ronchetti T (1988) J Mater Sci 23:459
32. Maspoch MLL, Ferrer-Balas D, Gordillo A, Santana OO (1999) J Appl Polym Sci 73:177
33. Paris PC, Tada H, Zahoor A, Ernst H (1979) In: Elastic-Plastic Fracture, ASTM Special Technical Publication No. 668, American Society of Testing and Materials, Philadelphia, PA, pp. 5–36
34. Bataille P, Boisse S, Schreiber HP (1987) Polym Eng Sci 27:622